Testing general relativity using the black hole mass gap

Maria Straight[a], Eric Baxter[b], Jeremy Sakstein[c]

[a]*Department of Engineering and Physics, Whitworth University, 300 W. Hawthorne Rd., Spokane, WA 99251*

[b]*Institute for Astronomy, University of Hawai'i, 2680 Woodlawn Drive, Honolulu, HI 96822*

[c]*Department of Physics and Astronomy, University of Hawai'i, Watanabe 416, 2505 Correa Road, Honolulu, HI 96822*

Abstract

The advent of gravitational-wave astronomy provides a new way to probe the mass distribution of stellar black holes. In this work we study the black hole mass gap to investigate whether this can be used to test modified gravity theories. Stellar structure theory predicts a gap in the mass distribution of stellar black holes around $50 - 150$ $M_\odot$ due to pair-instability supernova (PISN). In a PISN, electron-positron pairs reduce the pressure in a star and cause a violent explosion that leaves no black hole. We investigate the effects of modified gravity on the location of this mass gap by simulating the massive Population III progenitors of black holes with modified gravity. We demonstrate the power of this new test by finding a measurement of the gravitational constant $1 + \Delta G/G_{\rm N} = 0.98^{+0.06}_{-0.09}$ at 68% confidence. Upcoming LIGO O3 data is expected to improve the bounds on this constraint by roughly a factor of seven.

1. Introduction

The standard cosmological model assumes general relativity (GR) on all scales, but mysteries such as dark energy (Copeland et al., 2006), the cosmological constant problem (Burgess, 2015; Padilla, 2015), and tensions with the data such as the Hubble tension (see e.g. Knox and Millea (2020) and references therein) suggest that GR may break down on cosmological scales (Joyce et al., 2015; Koyama, 2016). Although GR has passed all experimental tests to date, it has not been tested on the largest scales at the same precision as within the solar system (Will, 2014; Berti et al., 2015; Koyama, 2016; Sakstein, 2018a,b; Baker et al., 2019).

Modified gravity theories challenge the assumptions of GR and provide a promising solution to these large-scale tensions (Desmond et al., 2019; Desmond and Sakstein, 2020). These models must satisfy constraints within the solar system while significantly changing gravity on cosmological scales. For modified gravity theories to explain large-scale mysteries such as dark energy while being experimentally viable, screening mechanisms such as the chameleon mechanism (Khoury and Weltman, 2004) and Vainshtein mechanism (Nicolis et al., 2009)

have been developed to hide modifications to gravity on small scales. These theories predict that the strength of gravity is very environment dependent, and this work investigates whether this prediction can be tested using the black hole mass gap.

Stellar structure theory predicts a black hole mass gap (BHMG), or an absence of black holes within a certain mass range, due to massive stars undergoing a pulsational pair-instability supernova (PPISN) (Rakavy and Shaviv, 1967; Fraley, 1968; Bond et al., 1984). Stars with masses $\gtrsim 45$ $M_\odot$ can potentially experience the pair-instability in which production of electron-positron pairs within the core destabilizes the star by reducing the pressure but not the density. Stars with helium cores between $M_{\rm He} \sim 30 - 60$ $M_\odot$ experience a pulsational pair instability (PPI) in which nuclear flashes cause a series of pulsations and mass ejections. While these pulsations are not energetic enough to disrupt the entire star, these stars eventually become unstable and collapse to form black holes that are less massive than the original stars because a significant fraction of the initial mass has been lost during pulsations. Stars with helium cores between $M_{\rm He} \sim 60-130$ $M_\odot$ are expected to be disrupted by pair-production, resulting in PISN that do not form black holes (Woosley, 2017; Marchant et al., 2018).

Current black hole observations are consistent with predictions from standard stellar models. Farmer et al. (2019) predicted the lower edge of the BHMG to be at 45 $M_\odot$. Gravitational-wave detections of binary black holes from the first two observing runs of the Laser Interferometer Gravitational-wave Observatory (LIGO) and Virgo have found a maximum black hole mass of $M_g = 50.2^{+16.2}_{-10.2}$ $M_\odot$ (Abbott et al., 2019a). Fishbach and Holz (2017) statistically measure the lower edge of the BHMG to be at about 41 $M_\odot$. Detections from the third LIGO/Virgo observing run are expected to significantly constrain the lower edge of the BHMG (Fishbach and Holz, 2017; Abbott et al., 2019b).

As LIGO has upgraded the sensitivity of its detectors and expects a significant increase in the number of detections in the coming O3 run and onward, now is an opportune time to consider how to use this new data to test gravity. The no-hair theorem (Mazur (2000) and references therein) implies that black holes behave the same in all theories of gravity, making it difficult to use black hole observations to test GR. This motivates studying the black hole progenitors and the location of the BHMG as we do in this work rather than individual black holes.

Stars are sensitive to modified gravity because they are held in equilibrium by a balance of pressure and gravity. Previous stellar structure tests using lower mass stars have successfully been used to constrain gravity (Sakstein, 2015). In this work, we test the effects of different values of the gravitational constant G on the evolution of massive stars. We numerically simulate the late evolutionary stages of massive stars under modified gravity and find that increasing G moves stars deeper into the instability region, which causes more mass loss and results in less massive black holes and lighter stars undergoing PISN. We test the effects of changing G on the location of the BHMG to discern how to constrain modified gravity theories using upcoming LIGO observations of binary black hole mergers.

This paper is organized as follows. In section 2, we explain our numerical methods. We

discuss the effects of changing G on individual stars and on the location of the BHMG from a grid of stars with different masses in section 3, and we explain our statistical methodology for finding a constraint on G. We conclude in section 4 by discussing possible systematics and future work.

2. Methods

We simulate black hole progenitors using version 12778 of the open-source MESA stellar evolution code (Paxton et al., 2011, 2018), modified to change Newton's gravitational constant $G_{\rm N}$ to $(1+\Delta G/G_{\rm N})G_{\rm N}$. Paxton et al. (2011) and Paxton et al. (2018) describe details about the MESA code and the PISN physics. Following the simulation procedure of Marchant et al. (2018) and Farmer et al. (2019), we evolve massive helium stars to core collapse or PISN. Changing G affects the hydrostatic equilibrium equation

$$\frac{{\rm d}P}{{\rm d}r} = -\frac{GM(r)}{r^2}\rho(r), \tag{1}$$

which determines the structure and evolution of the star; the escape velocity

$$v_{\rm esc}(r) = \sqrt{\frac{GM(r)}{r}}, \tag{2}$$

which affects the final mass as material with a velocity greater than $v_{\rm esc}$ is lost during pulsations; and the freefall timescale

$$t_{\rm f} = \frac{1}{\sqrt{G\rho}}, \tag{3}$$

which determines the time it take for the star to collapse. For greater values of G, the hydrostatic equilibrium equation causes raised temperatures at fixed mass, while increasing $v_{\rm esc}$ causes more material to remain bound. These competing effects make it difficult to know the combined effect of changing gravity a priori, so we use MESA to simulate the evolution of black hole progenitors under modified G.

2.1. Modifying MESA

We modify MESA to change the value of G for entire simulations. Individual pulses in a PPISN cause large fractions of the star's mass to be removed at high velocities, while the remaining material returns to hydrostatic equilibrium with a lower central temperature than before the pulse. MESA cannot compute the long-term evolution of both the ejected mass and the bound core, so the unbound layers are removed from the model and a new stellar model is relaxed using the procedure described in Appendix B of Paxton et al. (2018) such that it has the same mass, entropy, and composition profiles as the material that was bound in the hydrodynamical model. Appendix C of Marchant et al. (2018) explores how well

the relaxation procedure reproduces the pre-relaxation model. As a starting point for the relaxation, MESA calls pre-made stellar models of zero age main sequence (ZAMS) stars, but these models assume GR and are not in hydrostatic equilibrium for a different value of G. We generate new ZAMS models using the same specific values of G as our simulations to achieve hydrostatic equilibrium. Input files necessary to reproduce this work and the resulting output files will be made publicly available.

2.2. Locating the BHMG

For $1 + \Delta G/G_{\rm N}$ values of $0.90 - 1.10$ in steps of 0.1, we evolve a grid of helium stars below the BHMG with initial masses of $26 - 72$ $M_\odot$ with an interval of 1 $M_\odot$. Mass loss due to stellar winds is proportional to $(Z/Z_\odot)^{0.85}$, so higher metallicities imply greater mass loss (Vink et al., 2001; Brott et al., 2011). Because the lower edge of the BHMG in GR is found with metallicity $Z = 10^{-5}$, we use the same metallicity to find the maximum bound mass to collapse to a black hole for runs with modified gravity. Convection is modelled using mixing length theory (MLT) (Cox and Giuli, 1968) with efficiency parameter $\alpha_{\rm MLT} = 2.0$. Semi-convection is modeled using the same prescription as Langer et al. (1985) with efficiency parameter $\alpha_{\rm sc} = 1.0$. Convective over-shooting is described using an exponential profile parameterized by f_0, which determines the point where overshooting begins inside the convective boundary, and $f_{\rm ov}$, which determines the scale height of the overshoot. Following Farmer et al. (2019), we fix $f_0 = 0.005$ and $f_{\rm ov} = 0.01$.

We use the same physical definitions as previous studies Marchant et al. (2018) and Farmer et al. (2019). Helium depletion is defined as the time when the central helium mass fraction falls below 0.01. CO core masses are defined at core helium depletion as the innermost mass coordinate with a helium mass abundance greater than 0.01. The black hole mass is calculated as the mass bound within the outermost coordinate in which the layer's velocity is less than the escape velocity (Eq. 2). In the case where all layers have a velocity greater than the escape velocity, all of the mass becomes unbound in a pair-instability supernova (PISN) and no black hole is formed. The maximum black hole mass M_g to be formed by a star that does not explode in a PISN defines the lower edge of the BHMG.

3. Results and Discussion

According to analytic predictions (e.g. Eq. 36.4 in Kippenhahn et al. (2012)), increasing the value of G will cause an increase in the central temperature $T_{\rm c}$ at a fixed central density $\rho_{\rm c}$. Assuming radiation pressure domination and neglecting electron degeneracy pressure, the equation

$$\log_{10}(T_{\rm c}) = \frac{1}{3}\log_{10}(\rho_{\rm c}) + \log_{10} G + c, \tag{4}$$

where c is a constant, holds at fixed mass. Our results are consistent with this prediction. Figure 1 shows that increasing G raises the central temperature of the star at fixed density, which moves the star closer to the instability region. A greater instability will result in stronger pulsations and more mass loss, ultimately leading to a less massive black hole.

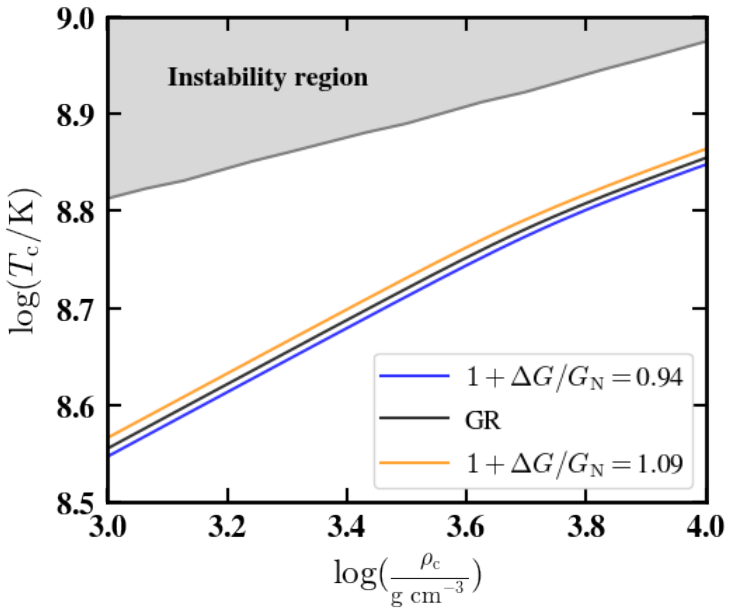

Figure 1: Central temperature vs. central density for a 56 $M_\odot$ star before undergoing pulsations. The shaded area represents the instability region due to electron-positron pair production. Increasing G (orange) moves the star closer to the instability, while decreasing G (blue) moves the star farther from the instability region.

3.1. Effects of modified gravity on the BHMG

Figure 2 shows the effects of increasing and decreasing the value of G on the masses of black holes formed for grids of stellar masses. As predicted, black holes are indeed less massive for increased values of G, and the resulting greater instability also causes lighter stars to undergo PISN. The converse is true when G is decreased as the reduced instability causes weaker pulsations so that less mass is lost. The right panel in Fig. 2 shows the source-frame component masses of 10 detections of binary black hole mergers observed by the LIGO and VIRGO detectors (Abbott et al., 2019a). Presented component masses represent median values with 90% credible intervals that include statistical and systematic errors from averaging the results of two waveform models for binary black holes. The redshift z is calculated from the luminosity distance assuming a standard flat ΛCDM cosmology with Hubble parameter $H_0 = 67.9$ km s^{-1} Mpc^{-1} and matter density parameter $\Omega_m = 0.306$. The physical binary masses in the source frame are computed by dividing the observed detector-frame masses by $(1 + z)$ (Abbott et al., 2019a). The shaded region shows the joint posterior (Eq. 12) for the lower edge of the BHMG calculated from the more massive black hole component of each of the ten LIGO detections. Figure 3 shows the maximum black hole mass found for each grid. The results, which spread across the joint posterior distribution calculated from LIGO detections, are used to constrain G in the next section.

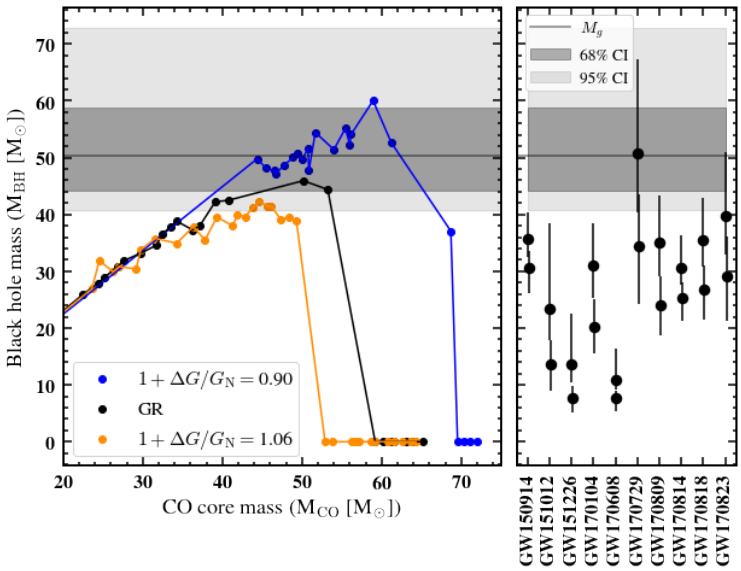

Figure 2: Black hole mass as a function of the star's carbon-oxygen (CO) core mass for metallicity $Z = 10^{-5}$. Black points show GR. The right panel shows component masses of binary black hole mergers detected by the first and second LIGO/VIRGO observing runs (Abbott et al., 2019a). Error bars show 90% confidence intervals on individual black hole masses. The shaded regions show 68% (darker) and 95% (lighter) confidence intervals for the joint posterior (Eq. 12) for the lower edge of the BHMG calculated from the more massive black hole component of each of the ten LIGO detections.

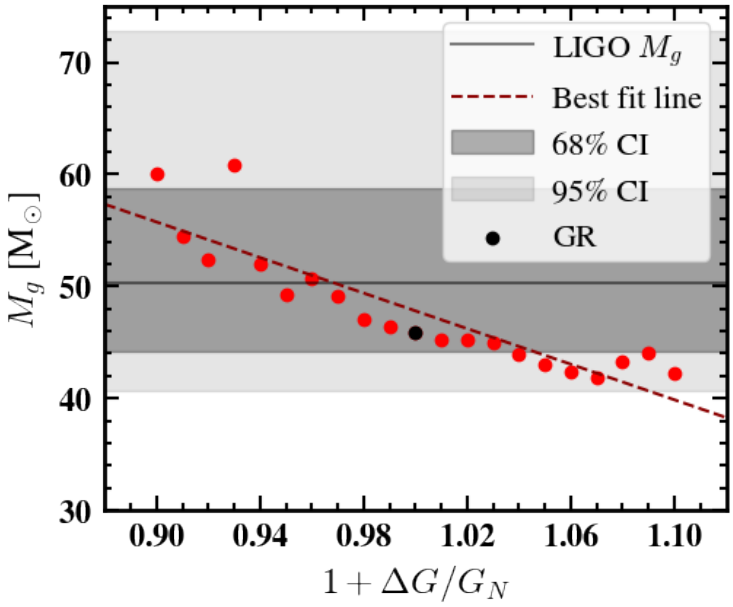

Figure 3: Maximum black hole mass M_g for each grid of masses with $G = (1 + \Delta G/G_N)G_N$ as a function of $1 + \Delta G/G_N$. Finer grids may find higher maximum black hole masses. The shaded regions show 68% (darker) and 95% (lighter) confidence intervals for the joint posterior (Eq. 12) for the lower edge of the BHMG calculated from the more massive black hole component of each of the ten LIGO detections. The equation for the best fit line (dashed) is given in Eq. 5.

3.2. Statistical methodology

We find a linear fit for our results in Fig. 3 that is given by the equation

$$\frac{M_g}{M_\odot} = -79\Big(1 + \frac{\Delta G}{G_{\rm N}}\Big) + 127. \tag{5}$$

Assuming this linear relationship between G and M_g, we use Bayesian methods to constrain G using LIGO observations.

For a single gravitational wave detection event d, LIGO reports a posterior on the BH mass $P_{\rm LIGO}(M|d) = P_{\rm LIGO}(d|M)P_{\rm LIGO}(M)$. LIGO adopts a uniform prior on M, so the likelihood is simply $P_{\rm LIGO}(d|M) = P_{\rm LIGO}(M|d)$. The posterior for M and M_g

$$P(M_g, M|d) \;=\; P_{\rm LIGO}(d|M)P(M|M_g)P(M_g) \tag{6}$$

follows from Bayes' theorem and the definition of conditional probability, where $P(M_g)$ is our prior on M_g, which we take to be flat. To constrain M_g, we marginalize over M:

$$P(M_g|d) \;=\; P(M_g)\int_0^{M_g} P_{\rm LIGO}(d|M)P(M|M_g)dM. \tag{7}$$

We calculate a simplified likelihood that assumes the black hole mass distribution is constant between a lower cutoff $M_{\rm min}$ (set at zero) and the maximum black hole mass M_g. Under this assumption, $P(M|M_g)$ is given as

$$\begin{aligned} P(M > M_g|M_g) &= 0 & (8)\\ P(M_{\rm min} < M < M_g|M_g) &= 1/(M_{\rm g} - M_{\rm min}) & (9)\\ P(M < M_{\rm min}|M_g) &= 0. & (10) \end{aligned}$$

Since LIGO assumes a uniform prior on M for the posterior parameter chains, the integral in Eq. 7 is given by a sum over the set of chain values, $\{M_i\}$:

$$\int_0^{M_g} P_{\rm LIGO}(d|M)P(M|M_g)dM = \frac{\sum_{M_i} P(M|M_g)}{\sum_{M_i} 1}. \tag{11}$$

A posterior is computed for each black hole measurement, and assuming each event is independent the combined constraint is computed as

$$P(M_g|d) \;=\; P(M_g)\prod_i \int_0^{M_g} P_{\rm LIGO}(d_i|M)P(M|M_g)dM \tag{12}$$

where we assume a uniform prior on M_g, i.e. $P(M_g) \propto$ constant. From the joint posterior for the ten LIGO detections, the maximum black hole mass for a 68% confidence interval

$M_g = 50.2^{+8.5}_{-6.0}$ $M_\odot$ is shown in the dark shaded region in Fig. 2. The probability of G is related to the probability of M_g by

$$P(G) \propto \frac{\mathrm{d}M_g}{\mathrm{d}G} P(M_g) \tag{13}$$

where $\mathrm{d}M_g/\mathrm{d}G$ is the Jacobian. For a linear relationship, the Jacobian is a constant equal to the slope of the best fit line (Eq. 5). Using these simplifying assumptions, we calculate the posterior probability $P(G|d)$ as a function of $1 + \Delta G/G_\mathrm{N}$ as shown in Fig. 4. We find $1+\Delta G/G_\mathrm{N} = 0.98^{+0.06}_{-0.09}$ for a 68% confidence interval and an upper limit of $1+\Delta G/G_\mathrm{N} < 1.07$ for a 95% confidence interval.

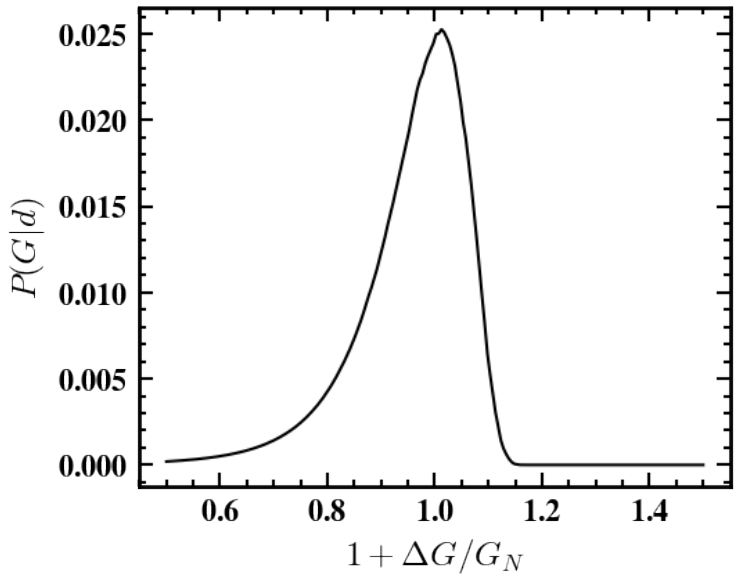

Figure 4: The posterior probability distribution of G gives $1 + \Delta G/G_\mathrm{N} = 0.98^{+0.06}_{-0.09}$ at 68% confidence.

4. Conclusions

Modified gravity theories provide a promising solution to cosmic mysteries such as the Hubble tension. We used simulations to study the effects of modified gravity on the location of the BHMG that exists due to pair-instability according to stellar structure theory. Our results shown in Fig. 3 indicate that greater values of G produce less massive black holes at the lower edge of the BHMG. Our simplified model used to obtain a measurement of G demonstrates that the BHMG can be used to test gravity using data from LIGO. Approximately $40 - 50$ new black hole detections expected in upcoming LIGO O3 data will probe the lower edge of the BHMG with higher precision, improving the constraint on G by an estimated factor of 7. The present analysis assumes a linear relationship between G and M_g and does not account for error bars on the best fit line. We will improve the analysis by testing this assumption,

accounting for errors, and using a more realistic likelihood specifically by accounting for a non-uniform distribution of black hole masses near the mass gap.

The location of the BHMG is sensitive to properties that affect stellar evolution such as metallicity, wind mass loss, and the $^{12}C(\alpha,\gamma)^{16}O$ reaction rate. The carbon to oxygen burning rate has an uncertainty rate of order 4 $M_\odot$, while the others give uncertainties of order 1 $M_\odot$. In future work, we will address these systematics by simulating grids with varying metallicities, wind mass losses, and nuclear reaction rates so that we can marginalize over the uncertainties. In this paper, we ignore stellar binarity, which will be important to study in follow-up work. Our preliminary study finds a $\sim$20 $M_\odot$ spread of M_g for the range of G values tested, which indicates a large signal and motivates further study. Future work will develop techniques to test the environmental dependence of G by cross-correlating the LIGO signal with galaxy cluster maps (Calore et al., 2020) or by using multimessenger observations with an electromagnetic counterpart to locate the source of the signal and better constrain modified gravity theories.

Acknowledgements

We are grateful to Robert Farmer, Pablo Marchant, and the MESA community for their help in answering our questions. MS acknowledges support from the Research Experience for Undergraduate program at the Institute for Astronomy, University of Hawai'i-Manoa funded through NSF grant 6104374. We would like to thank Robert Jedicke and the REU directors for their helpful feedback. MS would like to thank the Institute for Astronomy for their flexibility in hosting a remote REU during the COVID-19 pandemic.

References

B. Abbott et al. GWTC-1: A Gravitational-Wave Transient Catalog of Compact Binary Mergers Observed by LIGO and Virgo during the First and Second Observing Runs. *Phys. Rev. X*, 9(3):031040, 2019a. doi: 10.1103/PhysRevX.9.031040.

B. Abbott et al. Binary Black Hole Population Properties Inferred from the First and Second Observing Runs of Advanced LIGO and Advanced Virgo. *Astrophys. J. Lett.*, 882(2):L24, 2019b. doi: 10.3847/2041-8213/ab3800.

T. Baker et al. The Novel Probes Project – Tests of Gravity on Astrophysical Scales. 8 2019.

E. Berti et al. Testing General Relativity with Present and Future Astrophysical Observations. *Class. Quant. Grav.*, 32:243001, 2015. doi: 10.1088/0264-9381/32/24/243001.

J. R. Bond, W. D. Arnett, and B. J. Carr. The evolution and fate of Very Massive Objects. ApJ, 280: 825–847, May 1984. doi: 10.1086/162057.

I. Brott, S. E. de Mink, M. Cantiello, N. Langer, A. de Koter, C. J. Evans, I. Hunter, C. Trundle, and J. S. Vink. Rotating Massive Main-Sequence Stars I: Grids of Evolutionary Models and Isochrones. *Astron. Astrophys.*, 530:A115, 2011. doi: 10.1051/0004-6361/201016113.

C. Burgess. The Cosmological Constant Problem: Why it's hard to get Dark Energy from Micro-physics. In *100e Ecole d'Ete de Physique: Post-Planck Cosmology*, pages 149–197, 2015. doi: 10.1093/acprof:oso/9780198728856.003.0004.

F. Calore, A. Cuoco, T. Regimbau, S. Sachdev, and P. D. Serpico. Cross-correlating galaxy catalogs and gravitational waves: a tomographic approach. *Phys. Rev. Res.*, 2(2):2, 2020. doi: 10.1103/PhysRevResearch.2.023314.

E. J. Copeland, M. Sami, and S. Tsujikawa. Dynamics of dark energy. *Int. J. Mod. Phys. D*, 15:1753–1936, 2006. doi: 10.1142/S021827180600942X.

J. P. Cox and R. T. Giuli. *Principles of stellar structure*. 1968.

H. Desmond and J. Sakstein. Screened fifth forces lower the TRGB-calibrated Hubble constant too. *Phys. Rev. D*, 102(2):023007, 2020. doi: 10.1103/PhysRevD.102.023007.

H. Desmond, B. Jain, and J. Sakstein. Local resolution of the Hubble tension: The impact of screened fifth forces on the cosmic distance ladder. *Phys. Rev. D*, 100(4):043537, 2019. doi: 10.1103/PhysRevD.100.043537. [Erratum: Phys.Rev.D 101, 069904 (2020), Erratum: Phys.Rev.D 101, 129901 (2020)].

R. Farmer, M. Renzo, S. de Mink, P. Marchant, and S. Justham. Mind the gap: The location of the lower edge of the pair instability supernovae black hole mass gap. 10 2019. doi: 10.3847/1538-4357/ab518b.

M. Fishbach and D. E. Holz. Where Are LIGO's Big Black Holes? *Astrophys. J. Lett.*, 851(2):L25, 2017. doi: 10.3847/2041-8213/aa9bf6.

G. S. Fraley. Supernovae Explosions Induced by Pair-Production Instability. Ap&SS, 2(1):96–114, Aug. 1968. doi: 10.1007/BF00651498.

A. Joyce, B. Jain, J. Khoury, and M. Trodden. Beyond the Cosmological Standard Model. *Phys. Rept.*, 568: 1–98, 2015. doi: 10.1016/j.physrep.2014.12.002.

J. Khoury and A. Weltman. Chameleon cosmology. *Phys. Rev. D*, 69:044026, 2004. doi: 10.1103/PhysRevD.69.044026.

R. Kippenhahn, A. Weigert, and A. Weiss. *Stellar Structure and Evolution*. 2012. doi: 10.1007/978-3-642-30304-3.

L. Knox and M. Millea. Hubble constant hunter's guide. *Phys. Rev. D*, 101(4):043533, 2020. doi: 10.1103/PhysRevD.101.043533.

K. Koyama. Cosmological Tests of Modified Gravity. *Rept. Prog. Phys.*, 79(4):046902, 2016. doi: 10.1088/0034-4885/79/4/046902.

N. Langer, M. F. El Eid, and K. J. Fricke. Evolution of massive stars with semiconvective diffusion. A&A, 145(1):179–191, Apr. 1985.

P. Marchant, M. Renzo, R. Farmer, K. M. Pappas, R. E. Taam, S. de Mink, and V. Kalogera. Pulsational pair-instability supernovae in very close binaries. 10 2018. doi: 10.3847/1538-4357/ab3426.

P. O. Mazur. Black hole uniqueness theorems. 12 2000.

A. Nicolis, R. Rattazzi, and E. Trincherini. The Galileon as a local modification of gravity. *Phys. Rev. D*, 79:064036, 2009. doi: 10.1103/PhysRevD.79.064036.

A. Padilla. Lectures on the Cosmological Constant Problem. 2 2015.

B. Paxton, L. Bildsten, A. Dotter, F. Herwig, P. Lesaffre, and F. Timmes. Modules for Experiments in Stellar Astrophysics (MESA). *Astrophys. J. Suppl.*, 192:3, 2011. doi: 10.1088/0067-0049/192/1/3.

B. Paxton et al. Modules for Experiments in Stellar Astrophysics (MESA): Convective Boundaries, Element Diffusion, and Massive Star Explosions. *Astrophys. J. Suppl.*, 234(2):34, 2018. doi: 10.3847/1538-4365/aaa5a8.

G. Rakavy and G. Shaviv. Instabilities in Highly Evolved Stellar Models. ApJ, 148:803, June 1967. doi: 10.1086/149204.

J. Sakstein. Testing Gravity Using Dwarf Stars. *Phys. Rev. D*, 92:124045, 2015. doi: 10.1103/PhysRevD.92.124045.

J. Sakstein. Tests of Gravity with Future Space-Based Experiments. *Phys. Rev. D*, 97(6):064028, 2018a. doi: 10.1103/PhysRevD.97.064028.

J. Sakstein. Astrophysical tests of screened modified gravity. *Int. J. Mod. Phys. D*, 27(15):1848008, 2018b. doi: 10.1142/S0218271818480085.

J. S. Vink, A. de Koter, and H. J. Lamers. Mass-loss predictions for o and b stars as a function of metallicity. *Astron. Astrophys.*, 369:574–588, 2001. doi: 10.1051/0004-6361:20010127.

C. M. Will. The Confrontation between General Relativity and Experiment. *Living Rev. Rel.*, 17:4, 2014. doi: 10.12942/lrr-2014-4.

S. Woosley. Pulsational Pair-Instability Supernovae. *Astrophys. J.*, 836(2):244, 2017. doi: 10.3847/1538-4357/836/2/244.